Volume 9, Issue 3, 2019, 3949 - 3955 **ISSN 2069-5837**

Biointerface Research in Applied Chemistry

www.BiointerfaceResearch.com

https://doi.org/10.33263/BRIAC93.949955

Original Research Article **Open Access Journal**

Received: 16.05.2019 / Revised: 10.06.2019 / Accepted: 12.06.2019 / Published on-line: 15.06.2019

Realistic simulation of the polymers in inkjet process: the investigation of physical phenomena in the ejection of a droplet

Chanh Minh Thi Le [1, 2, *], Fatemeh Mollaamin [1], Dung My Thi Dang [1], Majid Monajjemi [1, 3], Chien Mau Dang [1]

[1]Institute for Nanotechnology (INT)– Vietnam National University - Ho Chi Minh city Community 6, Linh Trung Ward, Thu Duc District, Ho Chi Minh City, 700000, Vietnam.
[2]University of Science – Vietnam National University - Ho Chi Minh City 227 Nguyen Van Cu Street, ward 4, district 5, Ho Chi Minh City, 700000, Vietnam.
[3]Department of chemical engineering, Central Tehran Branch, Islamic Azad University, Tehran, Iran
*corresponding author e-mail address: ***ltmchanh@vnuhcm.edu.vn ; maj.monajjemi@iauctb.ac.ir***

ABSTRACT

Nowadays ink-jet printing technologies present a digitized printout of documents. Due to digital technology inkjet printing enables the production of any kind of images and between images - as an Analog printing process such as printing press does. The pressure waves in nozzle inlet are inflicted in this work for discussing the effects of pressure function on the dropped ejecting. Usually, the contractual and formal inkjet printing applied thermal (Piezo-activator) for generating droplets. But the electrostatic inkjet is most conventional compared to other methods. This work presents the basic approach to the modeling and simulation of the mechanism as well as how the comparison will be made with experimental data obtained at INT.

Keywords: *inkjet printing, digitized printout, ejection of a droplet.*

1. INTRODUCTION

Recently, the inkjet technology has been developed rapidly and investigated based on some physical phenomenon such as Piezoelectric-driven [1], actuating pressure [2], temperature and thermal bubble, electrostatic induced [3] and viscosity. These kind technologies have been developed from formal image printing to advanced technologies, as solar cells [4], Solder-Jet technology [5], sensors [6], color filter in flat panel display [7], Nano-powder suspension patterning [8] and various material processes [9]. Generally, inkjet printing technology is based on thermally or mechanically pushing out the liquids in the chamber through a nozzle via several actuators [10]. For ejecting a suitable droplet, various actuation method has been used which the thermal, pressure and piezoelectric actuation technologies commercially, are most important compared to other methods. Although economically, the thermal actuation is a general technique in this technology, the high temperature could damage the conductive nanoparticles dispersed in the inks [10]. Hence, the Piezoelectric-driven and actuating pressure considered to be favorable for the inkjet printing technology. Currently, conductive inkjet silver ink is used for investigating the drop micro pattern characteristic due to easy electrostatic induced inkjet printing in industrial compared to conventional technologies.

Obviously, developing manufacturing systems is being driven by those mentioned actuating, reductions in costs considering the environmental impact and automation. However, due to the restricted option of solutions, it is usually constructed by thin film deposition with the evaporation process through lithography which the processes are very intricate and expensive. Massive advantages can be obtained with using organic light emitting materials that can be deposited directly by inkjet printing methods. The polymer light emitting diodes (PLED) are by deposition through spin coating which is exclusive in manufacturing of single color. Via using inkjet printing technology, it is possible to deposit tiny pixels of red, green and blue elements for manufacturing the color filters with high resolution and low cost with simple processing [11,12]. Among the above mentioned systems, the actuations by piezoelectric and thermal bubble methods are most popular for the commercial inkjet printer. The ejection of liquid droplets through the nozzle is induced either by the displacement of a piezoelectric membrane that is matched with the liquid or by the formation of a vapor bubble in the ink via the heating of the non- inductive membrane. Due to the dispensing of polymer and liquid metals the unnecessary vaporization in the fluid section is an important advantage of piezoelectric inkjet printing. It is very favorable to have a prediction on how the liquid droplet is formed, ejected, and impacted on the substrate in a piezoelectric inkjet printing device for increasing the printing quality which is completely related to that of the ejected droplet. Therefore, with the simulating of these items, it is then feasible for controlling droplet size, droplet stability, via suitable designing of these kind instrument and fluids selection with such physical properties.

By this work Recently, the inkjet technology has been developed rapidly and investigated based on some physical phenomenon such as Piezoelectric-driven [1], actuating pressure [2], temperature and thermal bubble, electrostatic induced [3] and viscosity. These kind technologies have been developed from formal image printing to advanced technologies, as solar cells [4], Solder-Jet technology [5], sensors [6], color filter in flat panel display [7], Nano-powder suspension patterning [8] and various material processes [9]. Generally, inkjet printing technology is based on thermally or mechanically pushing out the liquids in the chamber through a nozzle via several actuators [10]. For ejecting a

suitable droplet, various actuations method has been used which the thermal, pressure and piezoelectric actuation technologies commercially, are most important compared to other methods. Although economically, the thermal actuation is a general technique in this technology, the high temperature could damage the conductive Nano-particles dispersed in the inks [10]. Hence, the Piezoelectric-driven and actuating pressure considered to be favorable for the inkjet printing technology. Currently, conductive inkjet silver ink is used for investigating the drop micro pattern characteristic due to easy electrostatic induced inkjet printing in industrial compared to conventional technologies.

By this work and based on physical phenomena in the ejection of a droplet, we have considered two important points in our simulation of the inkjet process, one how droplet is organized and second how droplet is impinged onto the layer.

For answering to these two points previous studies were accomplished for understanding the formation of a droplet by either bubbling or electro-static method. Initially, Bogy et al [13] investigated a model for calculating the temporary solution for the velocity and shape changing in a semi-infinite liquid pillar under the effects of periodic micro- perturbation of velocity at the nozzle. They presented a simultaneous finite difference solution of the nonlinear "Cosserat" Theory" fluid jet equations for a semi-infinite jet emanating from a circular nozzle. They exhibited in a low viscosity the jet breaks up into main drops of twice the nozzle diameter. In further works, Fromm et al. [14] simulated the shaping progress of ejected droplets via a driving pressure at the outlet of the nozzle while Asai [15] investigated a three-dimensional finite difference algorithm for solving "Navier-Stokes" equation to predict the drop ejection in a bubble jet printer. Chen et al. [16] designed and simulated a fluid dynamics simulation system for prediction the arc position with time inside an inkjet print head during the infusion and ejection stages. There has been no study on the simulation for the formation of a droplet with the actuation of piezoelectric-induced and thermal bubble based on a statically approach which has been investigated by this work.

1.1. Navier-Stokes Equation.

Navier–Stokes equations [17] are useful because they explain the non-classical physics of many phenomena of scientific and engineering research. They can be used to model and analyses the statically data of a weak flow in a pipe or drop ejection in a bubble jet printer. The solution of λ the Navier–Stokes equations is based on a flow velocity. Once the velocity situation is calculated other physical data, such as pressure or temperature, can be found through additional related equations. Studying velocity instead of position (which is used in classical mechanics) makes more sense for a fluid [18].

The Navier–Stokes momentum equation can be derived as a particular form of the Cauchy momentum equation, whose general convective form is $\rho\frac{Du}{Dt} = -\nabla P + \nabla.\tau + \rho g$ **(1)** where, $\frac{D}{Dt}$ is mathematical derivative, ρ is density, P is pressure, u is the flow velocity, "t" is time and τ is the stress tensor with order two this equation of momentum is important for simulating the dye-based inks which are used in some inkjet printing for diluting the polymer solution in water. This equation can be rewritten in view point of a comprisable flow or compressible momentum Navier–Stokes equation through Cauchy stress tensor as: $\sigma = \lambda(\nabla.u)I + 2\mu\varepsilon$ **(2)**, which "*I*" is the identity tensor and $\nabla.u$ is the rate of expansion flow and the trace of the stress tensor in three dimensions is shown as: Trace (σ)= $(3\,\lambda + 2\mu)\,\mu$**(3).** From the equations 2&3 second viscosity can be defined as: $\zeta \equiv \lambda + \frac{2}{3}\mu$ **(4).** Both dynamic viscosity (μ) and second viscosity (ζ) must be constant; usually both dynamic and second viscosities are related to the density. Although the viscosity is expressed through pressure, incompressible flows it would be interpreted by temperature [19]. Since the divergence of $\nabla\mathbf{u}$ & $(\nabla\mathbf{u})^{\mathrm{T}}$ tensors are$\nabla^2\mathbf{u}$ & $[\nabla(\nabla\cdot\mathbf{u})$ (known as Lamb Vector)] respectively, the most general Navier–Stokes momentum equation can be written as: $\rho\frac{Du}{Dt} = -\nabla\bar{P} + \mu\nabla^2\mathrm{u} + \frac{1}{3}\mu\nabla(\nabla.u) + \rho g$ **(5).** It is notable the volume viscosity "ζ" is a mechanical pressure and is not equal to a thermodynamic pressure which can be defined as $\bar{P} \equiv P - \zeta\nabla\mathrm{u}$ **(6).** To formulate the incompressible momentum Navier–Stokes equation it might be considered the Stokes' stress constitutive equation as $\tau = 2\mu\varepsilon$ where the rate-of-strain tensor is: $\varepsilon = 1/2(\nabla\mathbf{u} + (\nabla\mathbf{u})^{\mathrm{T}})$ then the Stokes's stress constitutive equation which only used for incompressible viscous fluids, is yielded as $\tau = \mu(\nabla\mathrm{u} + (\nabla\mathrm{u})^{\mathrm{T}})$ **(7).** Here the Dynamic viscosity μ might not be constant due to depending on density and also on pressure. Due to zero value for $\nabla\mathrm{u} = 0$ in an incompressible fluid, the incompressible momentum Navier–Stokes equation can be rewritten as: $\frac{\partial u}{\partial t} + (\mathbf{u}.\nabla)\mathbf{u} - \vartheta\nabla^2\mathrm{u} = -\nabla\omega + \mathbf{g}$. **(8)** which $\vartheta = \mu/\rho_0$ is kinematic viscosity [20]. There are five parts in the equation 8 (from left two rights) which indicate in terms of variation $(\frac{\partial u}{\partial t})$, conviction$(\mathbf{u}.\nabla)\mathbf{u})$, diffusion $(\vartheta\nabla^2\mathrm{u})$, internal source $(=-\nabla\omega)$ and external source $(\mathbf{g}.)$ respectively. The vector Laplacian "$\mu\nabla^2\mathbf{u}$**"** is the difference between the velocity at a point and the mean velocity in a small surrounding volume (it is an important physical parameter for inkjet printing) while this parameter implies the *diffusion of momentum*. So the incompressible Navier–Stokes equation leads to a vector diffusion which is named "Stokes equations", therefore incompressible Navier–Stokes equations are related to the series equation of convection-diffusion [19-21]. Vector operators are defined in terms of Del, including the gradient (∇), divergence $(\nabla.)$, and Curl $(\nabla\times)$. Using the curl of the Navier–Stokes equation yields a term in the removing of pressure. By assuming $u_z = 0$ the equation can be written as: $\rho(\frac{\partial u_x}{\partial t} + u_x\frac{\partial u_x}{\partial x} + u_y\frac{\partial u_x}{\partial y}) = -\frac{\partial p}{\partial x} + \mu\left(\frac{\partial^2 u_x}{\partial x^2} + \frac{\partial^2 u_x}{\partial y^2}\right) + \rho g_x$ **(9)**

$\rho(\frac{\partial u_y}{\partial t} + u_x\frac{\partial u_y}{\partial x} + u_y\frac{\partial u_y}{\partial y}) = -\frac{\partial p}{\partial y} + \mu\left(\frac{\partial^2 u_y}{\partial x^2} + \frac{\partial^2 u_y}{\partial y^2}\right) + \rho g_y$ **(10).**

The equations 9&10 describe the two dimensional of stream functions, where density unit (ρ) is $\mathrm{kgM^{-3}}$ and viscosity (μ) is Pascal second, meanwhile the unit of velocity "u" and Pressure (p) are $\mathrm{m.s^{-1}}$ and Pascal respectively. In addition g_y and g_x are the acceleration components due to gravity in y- and x-directions.

With defining a new parameter as stream function "Ψ" which is a definition for Incompressible flows in two dimensions as :$\{u_x = \frac{\partial \Psi}{\partial y}, u_y = \frac{\partial \Psi}{\partial x}\}$ and the conservation of mass for incompressible flow is:$\frac{\partial \Psi}{\partial y} + \frac{\partial \Psi}{\partial x} = 0$ **(11)**

1.2. Governing equations for polymers.

Diluted Polymers solutions in water are important inks for inkjet printing and their viscosities are the weakest parameter. Consequently it can be approximated through Newtonian fluids with suitable constant viscosities. Therefore these solvent inks are also incompressible fluid. Based on the Navier-Stokes (eq. 10), the velocities are constrained via the conservation of mass equation, which, for can be written as an incompressible flow$\nabla.\vec{V} = 0$. The decisive difficulties in simulation free surfaces flow is the estimating the location of free surfaces of the fluids and handling these free surfaces in view point of boundaries conditions. By the present work, the VOF (volume-of the Fluids) using Nichols and Hirt method [22] is applied for representing the fluids of polymers amplitudes for any further tracking and evolution of those boundaries. By the VOF, the function F(x, y, z, t) is defined for computing the volume fraction of polymer liquids in the particular cells. F=1 means the cell is completely full of liquids and F in F=0 cell is full of the gas without liquids. For any variable between 0 and 1, there are both liquids and gases with the interfaces.

1.3. Treatments for the free surface flow.

F is defined as equation: $\frac{\partial F}{\partial t} + (\overrightarrow{V}.\nabla)F = 0$ **(12)**. By solving this equation, F is soon smeared due to numerical diffusion and interfaces are no longer sharp. In addition, liquids volumes may not be conserved perfectly so, might be treated via other approaches. Several techniques have been illustrated for maintaining of a suitable definition for interfaces of volume fraction frameworks. Simple Line Interface Calculation or SLIC method investigated for dealing these situations of interfaces [23]. The SLIC interfaces demonstration is very harsh including many problems, especially when fewer deformations were involved. Another method is known as "Piecewise Linear Interface Calculation" or PLIC that has been investigated by Young [24], which yields an efficient refinement to the SLIC .The straight line is estimated through the liquid volumes in particular cells and also the adjacent cells. The PLIC method can be matched with the VOF method for any further advanced studies. As soon as the interfaces are combined or recombined, their motion via the velocities fields must be modeled through and an appropriate algorithm by either an Eulerian or a Lagrangian formula. Lagrangian computes directly the motion of the interfaces and also is matched in for further discussion. Consequently by the displacements of the planes, the F can be calculated through three steps. (1); constructs or reconstructs interfaces sheets. (2); solving the velocities equations. (3); updating F. Then for all determination of "F", a normal direction to the interfaces must be calculated for each surface's cell by $\vec{n} = \nabla F$ and then $-\vec{x}.\hat{n} - \alpha = 0$ **(13)** where α is a planer constant; $\vec{x}$ is a position vector and $\hat{n}$ is unit normalized vector. The mines sign explain the direction of the unit vector points towards the air. For the step 2, the flow fields $(U^*, \vartheta^*, \omega^*)$ at time steps of t^*(t +Δt), is confirmed and for cell faces including velocities of the $U^*, \vartheta^*, \omega^*$, approximate thickness of $U^*\Delta t, \vartheta^*\Delta t, \omega^*\Delta t$, is transported from the upstream to the downstream of cells during$[t^*, t]$. The volume transported of the liquids inside the layer, V_{adv}, is calculated through using reconstructed interfaces of Step1 (old time, t). For each cell, three contributions $\varphi^-_{ijk}, \varphi^+_{ijk}, \varphi^0_{ijk}$ can be calculated which the first and second item represent the volume fluxes, which enter the (i-1, j, k) and (i+1, j, k) cells, respectively, and the third item is the remained fluid volume in the (I, j, k) cell. The three volumes are shown in Fig. 1.

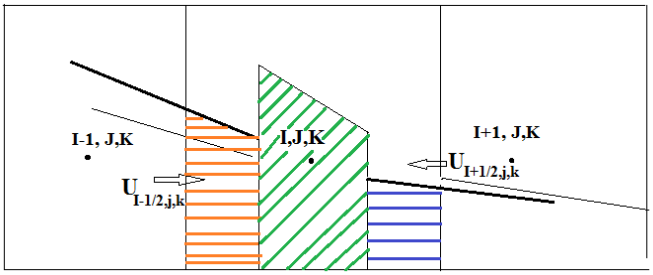

Figure1. Calculation of the volume fluxes during one fractional step

2. MATERIALS AND METHODS

2.1. Surface tension consideration for droplet.

The Fig.2 shows the surface curvature of a tiny and differential piece of a droplet surface under the equation of the Young–Laplace equation [24, 25]. Plateau-Rayleigh instability is a basic interpretation in continuous ink-jet printing process and is purely consequence of surface tension. The equation $\Delta P = \gamma(\frac{1}{R_x} + \frac{1}{R_y})$ is based on young-Laplace equation where γ is tension surface and R is radius of the drop in two direction of x and y. In order to calculate the amount of surface tension into a special boundary the Navier-Stokes equations at the interfaces must be used.

The surface tensions of different liquids are listed in Table 1. In a cylinder of liquid (Fig.3) there are two distinctive radii of curvature, which make differences in hydrostatic pressure - radius of the jet itself $R1$ and radius of curvature of the perturbation R_2. The total equation is; $R_z = R_0 + A_k\cos(kz)$, where R_z is the radius of the unperturbed stream of the axisymmetric jet (R_1) and A_k is the amplitude of the perturbation (R_2) and Z is distance along the axis of the stream while k is the wave number. Radius of the jet is always positive, so the pressure will be increase. The radius of curvature can also be negative, consequently decreasing the pressure completely in the region where radius of the jet is smaller. Via a Fourier's transformation, these kind perturbation can be change into sinusoidal functions as $R_z = R_0 + A_k\cos(kz)$whereA_k is small thanR_0, and $k = \frac{2\pi}{\lambda}$ where λ is the perturbation wave length. Perturbation amplitude is increasing until the drop finally pinches off from the stream of the jet. The most important property of jet breakup is satellite droplets which

are related between two steps of the string of liquids and starting to become drops. For estimating of these important points, one way is nonlinear analysis using a full numerical solution of the Navier-Stokes equation. The second alternative method is using a one-dimensional approximation to the jet equations [26].

Contact angle is one of the main subjects for a perfect simulation in a model of inkjet printing which is related to the surface of any liquids with an interface between those liquids and some other connectors. Obviously surface tension, is not alone property by itself, actually is a property of the liquid's interface with various connecters. For a container as a connector, there is also an interface between the liquid and the walls of the container.

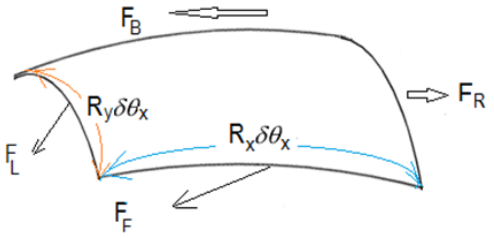

Figure2. Surface tension acting on a differential piece of Surface, $\delta\theta_x$ and $\delta\theta_y$ are the values of bending. Balancing the tension forces with pressure leads to The Young–Laplace equation

It is notable the surface tension between air and liquids is larger than its surface tension with the walls of a container [27, 28]. Based on this interpretation "θ" is defined as a contact angle between two places of surfaces media and liquids and calculated through vertical (F_v) and horizontal (F_h) forces (Fig.2) & Tables 1&2 [29]. Tension forces are shown for the liquid–air interface, the liquid–solid interface, and the solid–air interface.

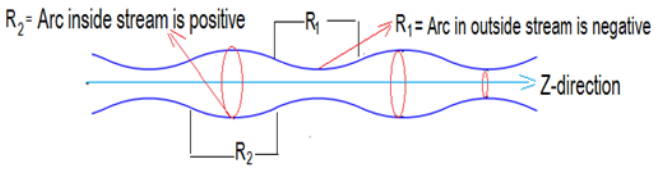

Figure3. Intermediate step of a jet breaking into droplets, Equation for the radius of the stream $R_z = R_0 + A_k\cos(kz)$, where R_z is the radius of the unperturbed stream of the Axisymmetric Jet (R_1) and A_k is the amplitude of the Perturbation (R_2) and Z is distance along the axis Of the stream while k is the wave number .

2.2. Continuous ink-jet and drop-on-demand.

Based the above equations and theoretical discussion, generally, ink-jet printing might be divided in two points of one, “continuous ink-jet approach”. And second “drop-on-demand”. The first item just described the mechanism of breaking up a jet’s liquid into the droplets through perturbation due to nozzle designing. In this work we have simulated the type of perturbation using several physical properties of the ink such as Piezoelectric-driven, actuating pressure, temperature (thermal bubble), electrostatic induced and viscosity. In our simulation we assumed the disturbance is depended to perturbation in radius, mechanical perturbation (piezoelectric) and thermal perturbation though, all mentioned methods finally lead to a perturbation in radius. It is notable that the amplitude of initial perturbation which we have used in our analysis now becomes just a proxy quantity that describes gross effect of nozzle setup and perturbation mechanism on the jet breakup (Fig.4).

Table1. Some liquid-solid angle [29]

Liquid	solid	Contact angle
Water	Fused quartz	0
Ethanol	Fused quartz	0
Diethyl ether	Fused quartz	0
Acetic acid	Fused quartz	0
water	silver	90
Methyl iodide	Fused quartz	33
Mercury	Soda-lime glass	140

Table2. Surface tension of various liquids in dyncm^{-1} against air [29]

Liquid	T °C	Surface tension
Water	0	75.64
Water	25	71.97
Water	50	67.91
Ethanol	20	22.27
Ethanol (40%) + Water	25	29.63
Ethanol (11.1%) + Water	25	46.03
Glycerol	20	63
***n*-Hexane**	20	18.4
Hydrochloric acid 17.7M aqueous solution	20	65.95
Isopropanol	20	21.7
Liquid Nitrogen	-196	8.85
Acetic acid	20	27.6
Acetic acid (40.1%) + Water	30	40.68
Acetic acid (10.0%) + Water	30	54.56
Acetone	20	23.7
Diethyl ether	20	17.0
Methanol	20	22.6
***n*-Octane**	20	21.8
Sodium chloride 6.0M aqueous solution	20	82.55
Sucrose (55%) + water	20	76.45
Mercury	15	487

3. RESULTS

The dimension of geometry is drawn in Fig. 4 with the related sizes depicted. The nozzle exit is 30 μ m in diameter. The nozzle interval to the substrate is 750 μm including deionized H2O as ink with surface tension in table 1 (75.64 dyncm^{-1} against air). Due to the densities and viscosities of the environmental gas are enough small compared to the liquid, there is less effect on this modelling. The maximum velocity is 10 m/s while the Reynolds number is around 300. The origin of operation of the piezoelectric inkjets print heading is based on the acoustic wave theories. The electrical induced piezoelectric condense the inks in connection with the converter, making an acoustic pressure pulses. Pressure pulses affect the fluid towards bottom

of the nozzle which can be changed through using several voltages. The experimental results of the droplets ejection caused via double voltages pulses might be discussed through the diffusion of acoustic pressure [30-43]. In a positive pressure, the arc at the nozzle is created and in other hand, the ejected droplet is disconnected from the nozzle in a negative pressure [44-50].

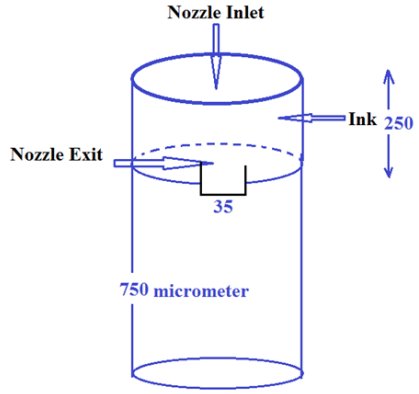

Figure 4. a schematic diagram of the inkjet print-head showing the nozzle configuration and dimensions of the simulated system.

The pressure waves in nozzle inlet are inflicted in this work for discussing the effects of pressure function on the dropped ejecting. The (+) amount of pressures are inflicted between 0 and t_1 and the negative amount is inflicted during t_1 to t_n. The breakings up of those droplets are completely observed in the range of t_1 to t_n. No more pressure is used after tn and the pressure pulses data have been tested in these fields, operating time and accelerated rate (Fig.5).

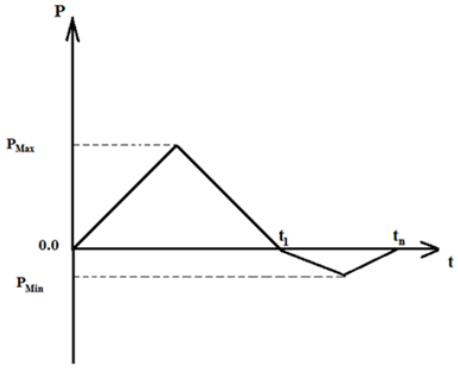

Figure5. Pressure-time relations at nozzle inlet.

3.1. Electrostatic ink-jetting

Usually, the contractual and formal inkjet printing applied thermal (Piezo-activator) for generating the droplets. But the electrostatic inkjet is most conventional compared to other methods. The fundamental configuration and model of the electrostatic inkjet scheme along with the forces during the droplet are shown in Fig.6 for any further studies.

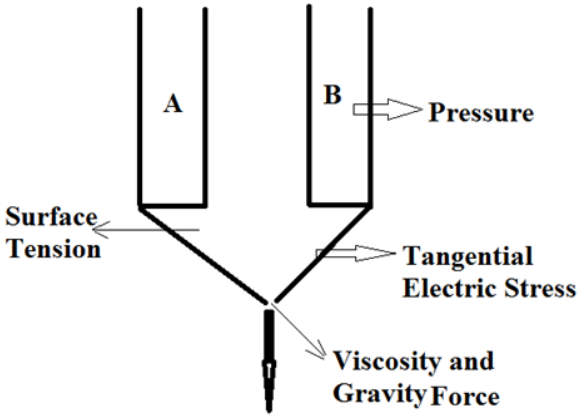

(a)

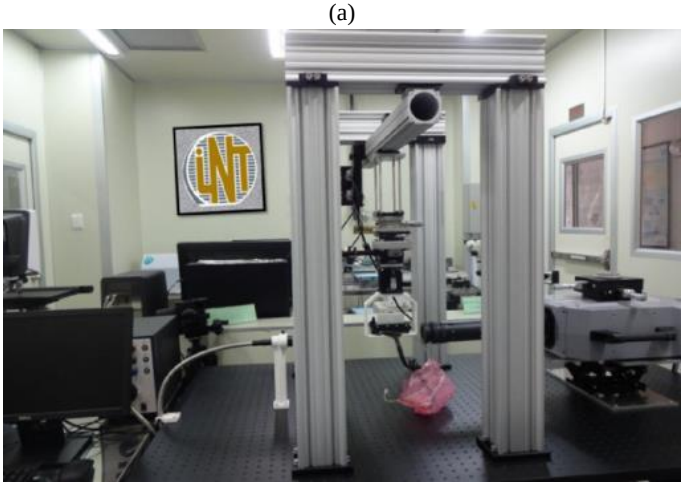

(b)

Figure6. (a) General Schematic of Electrostatic inkjet printing With Forces acting on the ink at the tip of the nozzle
(b) Real setup of the optical bench at INT for characterisation and simulation of the inkjet process

4. CONCLUSIONS

Nowadays ink-jet printing technologies present a digitized printout of documents. Due to digital technology inkjet printing enables the production of any kind of images and between images as analogy printing processes such as printing press does. DOD technologies have been pushed for its boundaries via h full-colour print speeds which this technology still has a lot of room for development. During a liquid ink droplet contacts the surface of a paper, it tends to spread along paper fibre lines as well as penetrating into paper pores. The spreading of ink droplets on paper could be too irregular to maintain the resolution required. The penetration of ink into the paper is usually too slow to absorb multiple ink drops on the same spot within very short time intervals. Poor colour image quality is due to ink inter colour mixing and surface flows of ink driven by pressure differences (due to differences in liquid film thickness) or by Marangoni flows (due to the presence of a gradient in surface tension).

5. REFERENCES

1. Guillou, O.; Daiguebonne, C.; Calvez, G.; Bernot, K. A long journey in lanthanide chemistry: From fundamental crystallogenesis studies to commercial anticounterfeiting taggants. *Acc. Chem. Res.***2016**, *49*, 844–856, https://doi.org/10.1021/acs.accounts.6b00058.

2. Wu, H.C.; Lin, H.J. The Japan Institute of Metals, Effect of Actuating Pressure Waveforms on the Droplet Behaviour in a Piezoelectric Inject. *Materials Transactions* **2010**, *51*, 2269–2276, http://dx.doi.org/10.2320/matertrans.M2010123.

3. Rahman, K.K; Ko, J.B.; Khan, S.; Kim, D.S.; Choi, K.H. Simulation of droplet generation through electrostatic forces.

Journal of Mechanical Science and Technology **2010**, *24*, 307-310, https://doi.org/10.1007/s12206-009-1149-y.
4. Hoth, C.N.; Choulis, S.A.; Schilinsky, P.; Brabec, C.J. High Photovoltaic Performance of Inkjet Printed Polymer:Fullerene Blends. *Adv. Mater.* **2007**, *19*, 3973–3978, https://doi.org/10.1002/adma.200700911.
5. Liu, Q.; Omre, M. High precision solder printing technology and the state-of-the-art. *J. Mater. Proc. Tech.* **2001**, *115*, 271–283, https://doi.org/10.1016/S0924-0136(01)00740-3.
6. Crowley, K.; O'Malley, E.; Morrin, A.; Smyth, M.R.; Killard, A.J. An aqueous ammonia sensor based on an inkjet-printed polyaniline nanoparticle-modified electrode. *Analyst* **2008**, *133*, 391–399, https://doi.org/10.1039/b716154a.
7. Koo, H.S.; Chen, M.; Pan, P.C. LCD-based color filter films fabricated by a pigment-based colorant photo resist inks and printing technology. *Thin Solid Films* **2006**, *515*,896–901, https://doi.org/10.1016/j.tsf.2006.07.159.
8. Tsai, M.H.; Hwang, W.S.; Chou, H.H.; Hsieh, P.H. Effects of pulse voltage on inkjet printing of a silver nano powder suspension. *Nanotechnology* **2008**, *19*, 304.
9. Singh, M.; Haverinen, H.M.; Dhagat, P.; Jabbour, G.E. Inkjet printing- Process and its application. *Adv. Mater* **2010**, *22*, 673–685, https://doi.org/10.1002/adma.200901141.
10. Le, H.P. Progress and Trends in Ink-jet Printing Technology. *Journal of imaging science and technology* **1998**, *42*, 49-62.
11. Hebner, T.R.; Wu, C.C.; Marcy, D.; Lu, M.H.; Strum, J.C. Ink-jet printing of doped polymers for organic light emitting devices. *Appl. Phys. Lett* **1998**, *72*, 519–521, https://doi.org/10.1063/1.120807.
12. Yamaguchi, K.; Sakai, K.; Yamanaka, T.; Hirayama, T. Generation of three-dimensional micro structure using metal jet. *Precision Eng* **2000**, *24*, 2–8, https://doi.org/10.1016/S0141-6359(99)00015-X.
13. Bogy, D.B.; Shine, S.J.; Talke, F.E. Finite difference solution of the Cosserat fluid jet equations. *J. Comput. Phys.* **1980**, *38*, 294–326, https://doi.org/10.1016/0021-9991(80)90151-5.
14. Fromm, J.E. Numerical calculation of the fluid dynamics of drop-on-demand jet. *IBM J. Res. Dev.* **1984**, *28*, 323–333, https://doi.org/10.1147/rd.283.0322.
15. Asai, A. Three-Dimensional Calculation of Bubble Growth and Drop Ejection in a Bubble Jet Printer. *J. Fluids Eng* **1992**, *114* , 638–641, https://doi.org/10.1115/1.2910079.
16. Liou, T.M.; Shih, K.C.; Chau, S.W.; Chen, S.C. Three-dimensional simulations of the droplet formation during the inkjet printing process. *Int. Comm. Heat Mass Transfer* **2002**, *29*, 1109–1118, https://doi.org/10.1016/S0735-1933(02)00439-6.
17. Roger, T. *Navier–Stokes Equations, Theory and Numerical Analysis*, AMS Chelsea**,** 2001; pp. 107–112.
18. Holdeman, J. T. A Hermite finite element method for incompressible fluid flow. *Int. J. Numer. Meth. Fluids* **2010**, *64*, 376– 408, https://doi.org/10.1002/fld.2154.
19. Holdeman, J.T.; Kim, J.W. Computation of incompressible thermal flows using Hermite finite elements. *Comput. Meth. Appl. Mech. Eng.* **2010**, *199*, 3297–3304, https://doi.org/10.1016/j.cma.2010.06.036.
20. Potter, M.; Wiggert, D.C. Schaum's Outlines, Fluid Mechanics, (Schaum's Series). *McGraw-Hill (USA)*, 2008.
21. Nunes, P.S.; Ohlsson, P.D.; Ordeig, O.; Kutter, J.P. Cyclic olefin polymers: Emerging materials for lab-on-a-chip applications. *Microfluid. Nanofluid* **2010**, *9*, 145–161, https://doi.org/10.1007/s10404-010-0605-4.
22. Hirt, C.W.; Nichols, B.D. Volume of fluid (VOF) method for the dynamics of free boundaries. *J. Comput. Phys* **1981**, *39*, 201–225, https://doi.org/10.1016/0021-9991(81)90145-5.
23. Keller, S.; Blagoi, G.; Lillemose, M.; Haefliger, D.; Boisen, A. Processing of thin SU-8 films. *J. Micromech. Microeng.* **2008**, *18*, 125020.
24. Youngs, D.L.; Time-Dependent Multi-material Flow with Large Fluid Distortion Fluid Dyn. *Academic Press* **1982**, 273–285.
25. Chemtob, A.; Ni, L.; Dietlin, C.; Croutxé-Barghorn, C.; Kitzmann, P.; Brogly, M.; Vidal, L. Spontaneous photoinduced formation of hybrid polymer films with functionalized macroporous patterns. *Surf. Coat. Technol.* **2012**, *209*, 64–72, https://doi.org/10.1016/j.surfcoat.2012.08.030.
26. Bousfield, D.W.; Keunings, R.; Marrucci, G.; Denn, M.M. Nonlinear Analysis of the Surface Tension Driven Breakup of Viscoelastic Filaments. *J. of Non-Newtonian Fluid mechanics* **1986**, *21*, 79–97, https://doi.org/10.1016/0377-0257(86)80064-7.
27. De Paz, H.; Chemtob, A.; Croutxé-Barghorn, C.; Le Nouen, D.; Rigolet, S. Insights into Photoinduced Sol-Gel Polymerization: An in Situ Infrared Spectroscopy Study. *J. Phys. Chem. B* **2012**, *116*, 5260–5268, https://doi.org/10.1021/jp212386e.
28. Baride, A.; Meruga, J.M.; Douma, C.; Langerman, D.; Crawford, G.; Kellar, J.J.; Cross, W.M.; May, P.S. A NIR-to-NIR upconversion luminescence system for security printing applications. *RSC Adv.* **2015**, *5*, 101338–101346, https://doi.org/10.1039/C5RA20785A.
29. Sears, F.W. Zemanski, M.W. *University Physics 2nd ed.* Addison Wesley, 1995.
30. Bao, B.; Li, M.; Li, Y.; Jiang, J.; Gu, Z.; Zhang, X.; Jiang, L.; Song, Y. Patterning fluorescent quantum dot nanocomposites by reactive inkjet printing. *Small* **2015**, *11*, 1649–1654, https://doi.org/10.1002/smll.201403005.
31. Wu, H.C.; Lin, H.J. Effects of Actuating Pressure Waveforms on the Droplet Behavior in a Piezoelectric Inkjet. *Materials Transactions* **2012**, *51*, 2269-2276, http://dx.doi.org/10.2320/matertrans.M2010123.
32. Lee, W.H.; Park, Y.D. Inkjet Etching of Polymers and Its Applications in Organic Electronic Devices. *Polymers* **2017**, *9*, 441, https://doi.org/10.3390/polym9090441.
33. Homola, T.; Shekargoftar, M.; Dzik, P.; Krumpolec, R.; Durasova, Z.; Vesely, M.; Cernak, M. Low-temperature (70 ◦C) ambient air plasma-fabrication of inkjet-printed mesoporous TiO2 flexible photoanodes. *Flex. Print. Electron.* **2017**, *2*, https://doi.org/10.1021/acsami.6b09556.
34. Sun, J.Z.; Guo, Y.Z.; Cui, B.; Chu, F.Q.; Li, H.Z.; Li, Y.; He, M.; Ding, D.; Liu, R.P.; Li, L.H.; Song, Y. Inkjet printing bendable circuits based on an oil-water interface reaction. *Appl. Surf. Sci.* **2018**, *445*, 391–397, https://doi.org/10.1016/j.apsusc.2018.03.204.
35. Sun, J.Z.; Yun, C.; Cui, B.; Li, P.; Liu, G.; Wang, X.; Chu, F. A Facile Approach for Fabricating Microstructured Surface Based on Etched Template by Inkjet Printing Technology. *Polymers* **2018**, *10*, 1209, https://dx.doi.org/10.3390%2Fpolym10111209.
36. Sun, J.Z.; Cui, B.; Chu, F.Q.; Yun, C.H.; He, M.; Li, L.H.; Song, Y.L. Printable nanomaterials for the fabrication of high-performance supercapacitors. *Nanomaterials* **2018**, *8*, 528, https://doi.org/10.3390/nano8070528.
37. Monajjemi , M.; Lee, V.S.; Khaleghian, M.; Honarparvar, B.; Mollaamin, F. Theoretical Description of Electromagnetic Nonbonded Interactions of Radical, Cationic, and Anionic

NH2BHNBHNH2 Inside of the B18N18 Nanoring. *J. Phys. Chem C* **2010**, *114*, 15315, http://dx.doi.org/10.1021/jp104274z.
38. Monajjemi, M.; Boggs, J.E. A New Generation of BnNn Rings as a Supplement to Boron Nitride Tubes and Cages. *J. Phys. Chem. A* **2013**, *117*, 1670-1684, http://dx.doi.org/10.1021/jp312073q.
39. 39. Samusjew, A.; Kratzer, M.; Moser, A.; Teichert, C.; Krawczyk, K.K.; Griesser, T. Inkjet Printing of Soft, Stretchable Optical Waveguides through the Photopolymerization of High-Profile Linear Patterns. *ACS Appl.Mater. Interfaces* **2017**, *9*, 4941–4947.
40. Bollgruen, P.; Gleissner, U.; Wolfer, T.; Megnin, C.; Mager, D.; Overmeyer, L.; Korvink, J.G.; Hanemann, T. Ink-jet printed fluorescent materials as light sources for planar optical waveguides on polymer foils. *Opt. Eng.* **2016**, *55*, 107107, https://doi.org/10.1117/1.OE.55.10.107107.
41. You, M.; Lin, M.; Wang, S.; Wang, X.; Zhang, G.; Hong, Y.; Dong, Y.; Jin, G.; Xu, F. Three-dimensional quick response code based on inkjet printing of upconversion fluorescent nanoparticles for drug anti-counterfeiting. *Nanoscale* **2016**, *8*, 10096–10104, https://doi.org/10.1039/c6nr01353h.
42. Alaman, J.; Alicante, R.; Pena, J.; Sanchez-Somolinos, C. Inkjet printing of functional materials for optical and photonic applications. *Materials* **2016**, *9*, 910, https://dx.doi.org/10.3390%2Fma9110910.
43. Parola, S.; Julian-Lopez, B.; Carlos, L.D.; Sanchez, C. Optical properties of hybrid organic-inorganic materials and their applications. *Adv. Funct. Mater.* **2016**, *26*, 6506–6544, https://doi.org/10.1002/9783527691036.hsscvol4023.
44. Sriramulu, D.; Turaga, S.P.; Yi, A.X.; Bettiol, A.A.; Valiyaveettil, S. Synthesis, characterization and application of luminescent silica nanomaterials. *J. Mater. Chem. C* **2016**, *4*, 11190–11197, http://dx.doi.org/10.1039/C6TC03677E.
45. Monajjemi, M. Non bonded interaction between BnNn (stator) and BN B (rotor) systems: A quantum rotation in IR region. *Chemical Physics* **2013**, *425*, 29-45, https://doi.org/10.1016/j.chemphys.2013.07.014.
46. Monajjemi, M.; Robert, W.J.; Boggs, J.E. NMR contour maps as a new parameter of carboxyl's OH groups in amino acids recognition: A reason of tRNA–amino acid conjugation. *Chemical Physics* **2014**, *433*, 1-11, https://doi.org/10.1016/j.chemphys.2014.01.017.
47. Monajjemi, M. Quantum investigation of non-bonded interaction between the B15N15 ring and BH2NBH2 (radical, cation, and anion) systems: a nano molecularmotor. *Struct Chem* **2012,** *23*, 551–580, http://dx.doi.org/10.1007/s11224-011-9895-8.
48. Monajjemi, M. Non-covalent attraction of B2N (2, 0) and repulsion of B2N (+) in the BnNn ring: a quantum rotatory due to an external field. *Theor Chem Acc* **2015**, 1668-9, https://doi.org/10.1007/s00214-015-1668-9.
49. Monajjemi, M. Metal-doped graphene layers composed with boron nitride–graphene as an insulator: a nano-capacitor. *Journal of Molecular Modeling* **2014**, *20*, 2507, https://doi.org/10.1007/s00894-014-2507-y.
50. M. Taufik, M.; Jain, P.K. Laser assisted finishing for improved surface finish of fused deposition modeled parts, *J. Manufacturing Processes*.**2017**, *30* , 161 - 177

6. ACKNOWLEDGEMENTS

This research is funded by FIRST Central Project Management Unit Grant Agreement No. 09/FIRST/2a/INT.